Lithos 368–369 (2020) 105596

Contents lists available at ScienceDirect

Lithos

journal homepage: www.elsevier.com/locate/lithos

Research Article

Phanerozoic magma underplating associated with remelting of the lower crust beneath the Cathaysia Block: Evidence from zircon U—Pb ages and Hf—O isotopes of granulite xenoliths from Daoxian, South China

Ying Wei [a,b], Xiao-Long Huang [a,*], Yang Yu [a], Xue Wang [a], Peng-Li He [a], Wan-Wei Ma [a]

[a] State Key Laboratory of Isotope Geochemistry, Guangzhou Institute of Geochemistry, Chinese Academy of Sciences, Guangzhou 510640, China
[b] State Key Laboratory of Nuclear Resources and Environment, East China University of Technology, Nanchang 330013, China

ARTICLE INFO

Article history:
Received 10 February 2020
Received in revised form 22 May 2020
Accepted 23 May 2020
Available online 30 May 2020

Keywords:
Granulite xenolith
Zircon Hf—O isotopes
Magma underplating
Crustal remelting
Lower crust
Cathaysia Block

ABSTRACT

Widespread Mesozoic granitoids in the Cathaysia Block of South China are associated with intensive reworking of the lower crust as a result of magma underplating. This inference is based mainly on studies of mafic igneous rocks, whereas there is little evidence from lower-crustal rocks. Lower-crustal xenoliths in Mesozoic basalts in the Daoxian region within the Cathaysia Block might record information on the relationship between magma underplating and remelting of the pre-existing crust beneath the block. The xenoliths are mainly mafic granulites, with minor felsic granulites. The mafic granulites have low SiO_2 contents (47.22–49.46 wt%) and high Mg# values (77.8–82.4), suggesting that their protoliths were derived from a mantle source. The felsic granulite xenoliths have high SiO_2 (69.56–70.27 wt%) and low MgO (1.63–2.50 wt%) contents, and zircons in these xenoliths yield negative $\varepsilon_{Hf}(t)$ values (−6.1 to −12.6) and high $\delta^{18}O$ values (6.8–7.6‰), consistent with a crustal source. Both mafic and felsic granulite xenoliths record magmatic (226–218 Ma) and metamorphic (218–193 Ma) events, suggesting a genetic link between mafic and felsic rocks in the lower crust. We propose that the magma underplating was responsible for the origin of the mafic granulites and partial melting of pre-existing lower crust, as recorded by the felsic xenoliths. The granulite xenoliths also contain abundant inherited zircons that formed during the Archean–Neoproterozoic (2584–659 Ma), early Paleozoic (peaking at ca. 425 Ma), and late Paleozoic (peaking at ca. 261 Ma). Zircons from the Daoxian granulite xenoliths have distinct Hf—O isotopic compositions that record the multistage evolution of the lower crust beneath the Cathaysia Block. This evolution involved the accretion of juvenile crust during the late Archean ($\varepsilon_{Hf}(t) = +4.2$ to $+4.6$) and late Paleozoic ($\varepsilon_{Hf}(t) = +1.3$ to $+5.3$; $\delta^{18}O = 5.8–6.2‰$), crustal reworking during the Neoproterozoic ($\varepsilon_{Hf}(t) = -7.5$ to -11.8; $\delta^{18}O = 5.1–9.5‰$) and early Paleozoic ($\varepsilon_{Hf}(t) = -0.5$ to -2.2; $\delta^{18}O = 7.3–7.5‰$), and crustal accretion with significant reworking during the early Mesozoic ($\varepsilon_{Hf}(t) = -19.2$ to $+5.9$; $\delta^{18}O = 6.8–7.6‰$). The U—Pb ages and Hf—O isotopic data of zircons from the Daoxian granulite xenoliths are consistent with the distribution of Phanerozoic igneous rocks in the Cathaysia Block. These data support the inference that Mesozoic magma underplating triggered the remelting of pre-existing crustal materials and produced extensive granitoid magmatism.

1. Introduction

Underplating by mantle-derived magma is a key mechanism of lower continental crustal growth (Fyfe, 1992; Rudnick, 1995). Granulite xenoliths record this process because they represent samples of in situ lower crust with a range of ages and origins (e.g., Downes et al., 2007; Moyen et al., 2017; Zheng et al., 2009). Except for fragments of ancient lower crust and the residues after remelting (Jiang et al., 2011; Jiang and Guo, 2010), most mafic granulite xenoliths accumulated in the lower crust through magma underplating and subsequently underwent granulite facies metamorphism during the Phanerozoic (e.g., Downes et al., 2007; Fan et al., 2005; Huang et al., 2001; Liu et al., 2010; Zhou et al., 2002). Younger felsic granulite xenoliths, on the other hand, are generally interpreted as being partial-melting products of pre-existing lower crust (Jiang et al., 2011; Wei et al., 2015). Magma underplating usually results in the formation of a juvenile crust represented by mafic granulite xenoliths, which may be distinctly younger than granulite terrains (e.g., Downes et al., 2007; Huang et al., 2004; Zheng et al., 2009). Meanwhile, magma underplating frequently induces remelting and even differentiation of the lower crust (Fountain, 1989; Ma et al., 2012; Thybo and Artemieva, 2013). Hence granulite xenoliths record the genetic relationship between mantle-derived magma underplating and remelting of the lower crust.

* Corresponding author.
E-mail address: xlhuang@gig.ac.cn (X.-L. Huang).

https://doi.org/10.1016/j.lithos.2020.105596
0024-4937/

Previous studies have proposed that the widespread Mesozoic granitoids in the Cathaysia Block resulted from partial melting of the middle–lower crust (e.g., Gao et al., 2017; Wang et al., 2007, 2011; Zhou et al., 2006) and that underplating by mantle-derived magma might provide necessary heat and material for the granitoid magmatism (Li et al., 2009; Zhou and Li, 2000). In contrast, the Cathaysia Block contains scare Mesozoic mantle-derived rocks, including mafic granulite xenoliths, basalts, gabbros, and mafic microgranular enclaves (MMEs) in felsic igneous rocks. Previous studies have reported that the origin of granulite xenoliths carried by Cenozoic or Mesozoic basalts in the southeastern part of the Cathaysia Block was related to magma underplating involving variable amounts of crustal material (e.g., Dai et al., 2008; Huang et al., 2013a; Li et al., 2018; Xu et al., 1999; Yu et al., 2003a). Therefore, a detailed study of the granulite xenoliths is crucial to understanding the connection between magma underplating and remelting of pre-existing crust. Such study, when combined with geochronological and geochemical data for the Phanerozoic granitoids in the Cathaysia Block, would provide valuable insights into the accretion and reworking history of the lower crust.

The early Mesozoic basalts in the Daoxian County, Cathaysia Block (Fig. 1), contain abundant mantle and lower-crustal xenoliths (e.g., Dai et al., 2008; Li et al., 2018; Zheng et al., 2004). These xenoliths yield ages from Archean to Mesozoic (Dai et al., 2008; Li et al., 2018), and may record thermal events contemporaneous with the widespread Paleozoic–Mesozoic granitoid magmatism in the Cathaysia Block. In this paper, we present whole-rock major element contents and in situ zircon U—Pb ages and Hf—O isotopic compositions of the Daoxian granulite xenoliths , with aims to determine the Phanerozoic evolution of the lower crust beneath the Cathaysia Block, which might improve our understanding of the genetic relationship between magma underplating and remelting of the lower crust.

2. Geological background and sampling

The South China Block includes the Yangtze Craton to the northwest and the Cathaysia Block to the southeast (Fig. 1). The basement of the Yangtze Craton contains mainly widespread Archean–Paleoproterozoic rocks (e.g., Xiang et al., 2018; Zhao and Cawood, 2012; Zheng et al., 2006) covered by Neoproterozoic igneous and sedimentary rocks, and Paleozoic and lower Mesozoic strata (e.g., Chen et al., 2018; Yan et al., 2003; Zhao et al., 2018). In the Cathaysia Block, the oldest exposed rocks are Paleoproterozoic, but detrital and xenocrystic zircon ages (3.7–2.5 Ga) suggest crustal growth during the Archean (e.g., Li et al., 1989; Xu et al., 2007; Zheng et al., 2011). The basement of the Cathaysia Block is mainly Neoproterozoic rocks covered by early Paleozoic deposits (Li et al., 2010; Wan et al., 2010; Yu et al., 2010). The Cathaysia Block records intensive and widespread felsic magmatism with peak periods during the Caledonian (early Paleozoic), Indosinian (Triassic), and Yanshanian (Jurassic–Cretaceous) (e.g., Li et al., 2003; Li and Li, 2007; Shu et al., 2015; Wang et al., 2011, 2013; Zhou et al., 2006). In contrast, outcrops of contemporaneous basalts and intrusive mafic rocks are scarce in the Cathaysia Block.

Basalts in the Daoxian region (^{40}Ar—^{39}Ar plateau age of 154–149 Ma; Li et al., 2004) were erupted close to the suture zone between the Yangtze Craton and the Cathaysia Block. The basaltic lavas

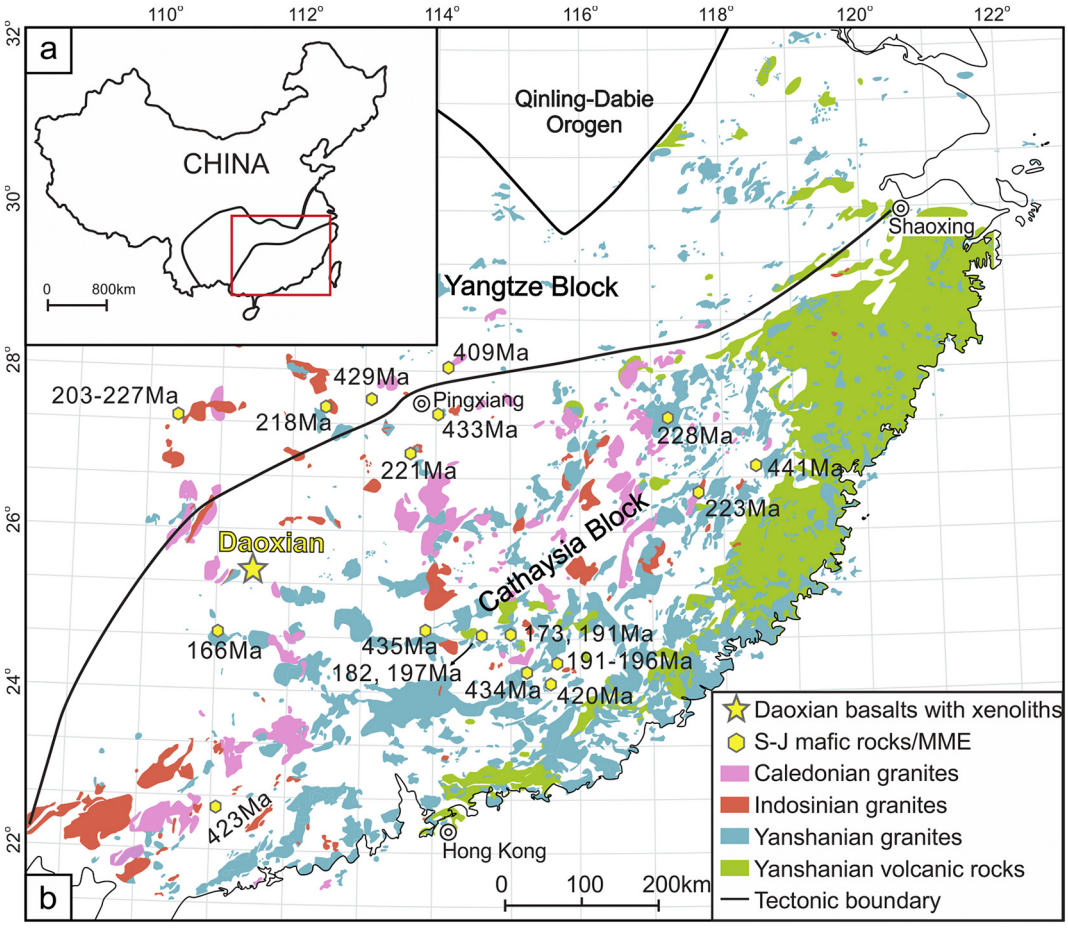

Fig. 1. Simplified geological map of the South China Block (modified from Wang et al., 2011; Zhou et al., 2006) showing the locations of the reported mafic rocks (Chen et al., 2007; Gan et al., 2017; Jiang et al., 2015; Wang et al., 2013, 2015; Yao et al., 2012; Zhang et al., 2015; Zhong et al., 2013).

carried abundant mantle and lower-crustal xenoliths (e.g., Dai et al., 2008; Li et al., 2018; Zheng et al., 2004). Petrographic observation and pressure-temperature estimates suggest that most of the Daoxian granulite xenoliths accumulated in the lower crust (Dai et al., 2008; Li et al., 2018). Thus, these xenoliths might provide information on the evolution of the lower crust beneath the Cathaysia Block.

Samples collected for this study include 11 mafic and 2 felsic granulite xenoliths with a range of shapes and sizes, 5–20 cm in diameter. The mafic xenoliths comprise mainly two-pyroxene granulites and one composite sample (DHZ16). They contain clinopyroxene (20–40%), orthopyroxene (15–35%), and plagioclase (20–50%) as primary mineral phases (Fig. 2a). Spinels (<5%) occur as a vermicular exsolution phase (Fig. 2b) and as inclusions within the pyroxenes or along their grain boundaries. Some samples contain minor (<1%) olivine, amphibolite, and rutile. The two-pyroxene granulite samples are medium-grained and display a granoblastic texture defined by plagioclase and pyroxene with triple junction grain boundaries. The composite sample DHZ16 has a granoblastic texture similar to that of the two-pyroxene granulite samples and displays a partially preserved ophitic texture. Clinopyroxene and plagioclase crystals that define the ophitic texture are tabular, 1–2 mm long, and <1 mm wide, and might represent relict crystals of a metamorphic event (Fig. 2c). The felsic granulite samples are medium–coarse-grained and display a granoblastic texture defined by plagioclase and pyroxene with triple junction grain boundaries (Fig. 2d). They comprise mainly plagioclase (60–80%) and lesser amounts of clinopyroxene (10–20%) and orthopyroxene (10–20%). Plagioclase grains are larger than pyroxene grains. Previous studies have reported that mafic xenoliths have high Mg# values, and are enriched in LREE and depleted in HFSE (Dai et al., 2008; Li et al., 2018). Furthermore, the whole-rock Sr—Nd isotopic compositions of the mafic granulite xenoliths suggest that their source was derived from the mixing of depleted mantle end-member and enriched end-member such as lower crustal component.

3. Analytical methods

The whole-rock major element compositions were analyzed using the Shimadzu XRF-1800 sequential X-ray fluorescence spectrometer at China University of Geosciences (Wuhan). The instrument model and operating conditions are given in Ma et al. (2012). The USGS standard BHVO-2 and Chinese national standard GSR-1 were used to monitor the data quality and the analytical uncertainties are better than 3%.

In-situ zircon U—Pb ages and Hf—O isotopic compositions were measured at State Key Laboratory of Isotope Geochemistry, Guangzhou Institute of Geochemistry, Chinese Academy of Sciences. Cathodoluminescence (CL) images of the zircons were obtained using field emission scanning electron microscopy (Supra 55 Sapphire) to characterize the internal structures. Zircon U—Pb dating was performed on a Cameca IMS-1280HR ion microprobe following the procedures of Li et al. (2009). An O_2^- primary ion beam with an intensity of 10 nA was accelerated at 13 kV, and the ellipsoidal spot was approximately $20 \times 30\ \mu m^2$. Positive secondary ions with a 10 kV potential were extracted. Correction of the Pb/U fractionation was based on an observed linear relationship between $\ln(^{206}Pb/^{238}U)$ and $\ln(^{238}U^{16}O_2/^{238}U)$. The measured compositions were corrected for common Pb. Plešovice zircon was used as an external standard, and Qinghu zircon was used as the unknown to monitor the data quality of the U—Pb dating. To test the zircon O isotopes, a Cs^+ primary ion beam with an intensity of ~2–3 nA was accelerated at 10 kV. The spot was approximately 20 μm in diameter. The operating conditions, analytical procedure, data calibration and monitoring are described in detail by Yang et al. (2018). The zircon Lu—Hf isotopes were analyzed by multiple-collector

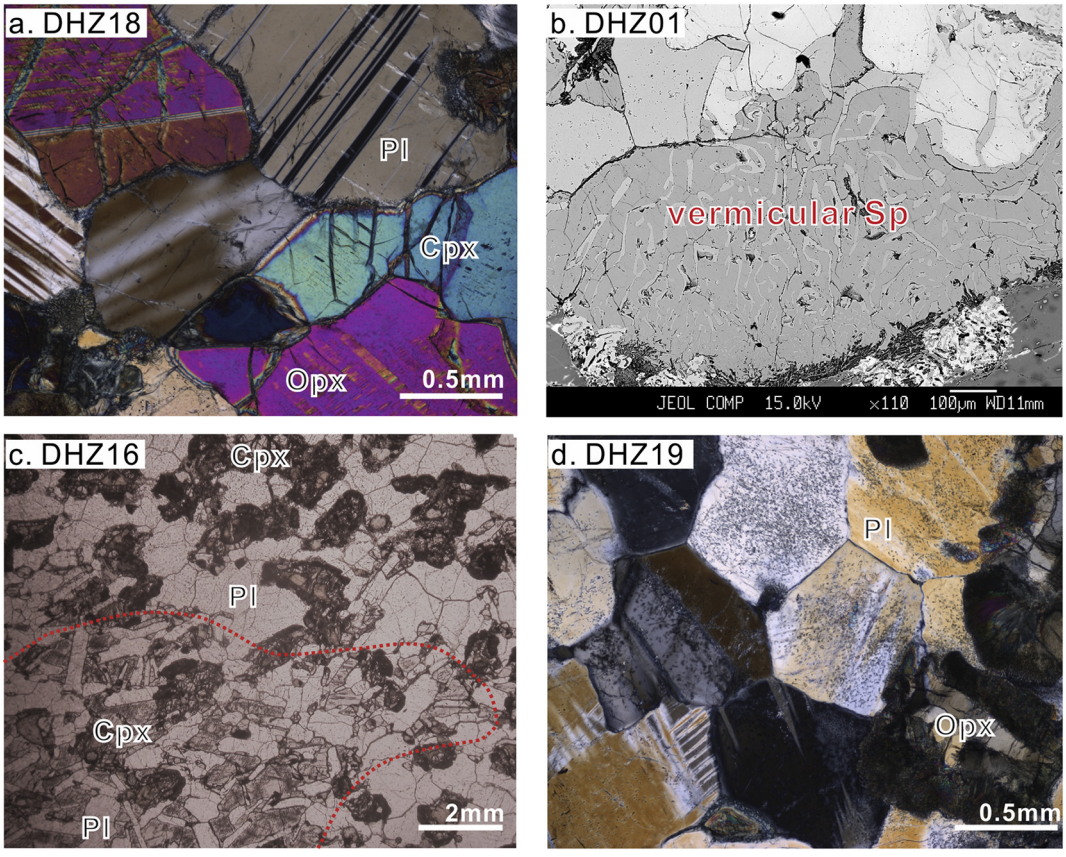

Fig. 2. Photomicrographs of the Daoxian granulite xenoliths: (a) mafic granulite (cross-polarized light); (b) spinel inclusions in mafic granulite (BSE); (c) relict ophitic texture in mafic granulite (plane-polarized light); (d) triple junction of plagioclase in felsic granulite (cross-polarized light). Cpx, clinopyroxene; Opx, orthopyroxene; Pl, plagioclase; Sp, spinel.

inductively coupled plasma mass spectrometry (Neptune Plus) and a RESOlution M-50193 nm laser ablation system. The zircon standard Penglai was used to monitor the measurement procedures and data quality.

4. Results

The major-element compositions of the Daoxian granulite xenoliths and their zircon U—Pb ages and Hf—O isotopic compositions are provided in Supplementary Tables S1–S3.

4.1. Whole-rock major elements

The mafic granulite samples have low SiO_2 (47.22–49.46 wt%) and alkali ($Na_2O + K_2O$ = 1.86–3.54 wt%) contents, and high Al_2O_3 (15.43–21.41 wt%), TFe_2O_3 (4.21–6.72 wt%), and MgO (8.60–13.70 wt%) contents; their Mg# values are high at 77.8–82.4 (Supplementary Table S1). The two felsic granulite samples have high SiO_2 (69.56–70.27 wt%), Al_2O_3 (13.00–14.22 wt%), and alkali ($Na_2O + K_2O$ = 6.38–8.69 wt%) contents and low TFe_2O_3 (1.83–3.18 wt%) and MgO (1.63–2.50 wt%) contents. Their Mg# values (60.9–63.8) are lower than those of the mafic granulite samples.

4.2. Zircon U—Pb ages and Hf—O isotopes

4.2.1. Mafic granulite sample DHZ14

Zircons from the mafic granulite DHZ14 occur as anhedral grains with round to elongate shapes. In CL images, they show oscillatory zoning (Fig. 3a), indicating a magmatic origin. Twenty-nine U—Pb analyses of 25 zircons indicate highly variable U (25–411 ppm) and Th (6–400 ppm) contents with Th/U ratios of 0.02–1.12 (Supplementary Table S2). Cores and rims were analyzed in four zircons (spots 5, 8, 17 and 19), yielding similar U—Pb ages (Supplementary Table S2). All zircons have $^{207}Pb/^{206}Pb$ or $^{206}Pb/^{238}U$ ages of 1191 ± 35 to 216 ± 4 Ma, and some show discordant data (Fig. 4a). Spots 19r, 49, 20 and 45 on concordant zircons yield $^{206}Pb/^{238}U$ ages of 750 ± 11, 685 ± 10, 659 ± 9 Ma and 358 ± 6 Ma, respectively. The remaining concordant zircons can be divided into three clusters, with weighted mean $^{206}Pb/^{238}U$ ages of 425 ± 6 Ma (MSWD = 1.2, n = 4), 261 ± 3 Ma (MSWD = 0.96, n = 7), and 218 ± 4 Ma (MSWD = 0.25, n = 3). Sixteen in situ O isotopic analyses were performed on 13 zircons. The $\delta^{18}O$ values of late Paleozoic zircons and one late Triassic zircon (5.8–6.2‰) are lower than those of early Paleozoic zircons (7.3–7.5‰), whereas Neoproterozoic–Mesoproterozoic zircons yield variable $\delta^{18}O$ values (5.1–9.5‰; Supplementary Table S3). Sixteen in situ Hf isotopic analyses were performed on the same sites as those analyzed for U—Pb dating. The zircons have variable $^{176}Hf/^{177}Hf$ ratios of 0.281849–0.282766, corresponding to $\varepsilon_{Hf}(t)$ values of −19.2 to +6.8 (Supplementary Table S3). Late Triassic zircons have negative $\varepsilon_{Hf}(t)$ values of −4.8 to −19.2; while late Paleozoic zircons have positive $\varepsilon_{Hf}(t)$ values of +1.3 to +5.3, except for one zircon grain with an age of 358 ± 6 Ma and an $\varepsilon_{Hf}(t)$ value of −15.3 (Supplementary Table S3). Most early Paleozoic zircons exhibit negative $\varepsilon_{Hf}(t)$ values of −0.5 to −2.2, except for one analysis (spot 46) with a high $\varepsilon_{Hf}(t)$ value of +6.8. Neoproterozoic–Mesoproterozoic zircons yield negative $\varepsilon_{Hf}(t)$ values of −7.5 to −11.8.

4.2.2. Mafic granulite sample DHZ16

Zircons from the mafic granulite DHZ16 occur as anhedral grains. One zircon displays weak oscillatory zoning, while the others display uniform internal structures (Fig. 3b). Seven U–Pb–O isotopic analyses were performed on six zircons and five Hf isotopic tests were conducted on the same sites for U—Pb dating. The zircons have a wide range of Th (13–657 ppm) and U (14–874 ppm) contents with Th/U ratios of 0.27–0.90 (Supplementary Table S2). Three old discordant analyses (spots 3, 7r and 9) yield a range of $^{207}Pb/^{206}Pb$ apparent ages from 2272 ± 10 Ma to 2442 ± 20 Ma, whereas old concordant zircon analyses (spots 7c and 5) yield similar $^{207}Pb/^{206}Pb$ apparent ages of 2584 ± 14 and 2568 ± 13 Ma but very different $\delta^{18}O$ values of 4.7‰ and 8.1‰. The old zircons (spots 5, 7c and 9) exhibit positive $\varepsilon_{Hf}(t)$ values of +0.6 to +4.6. In contrast, two young concordant zircons (spots 2 and 1) yield different $^{206}Pb/^{238}U$ apparent ages of 275 ± 4 and 221 ± 3 Ma (Fig. 4b), similar $\delta^{18}O$ values of 5.9‰ and 6.2‰, and negative $\varepsilon_{Hf}(t)$ values of −12.4 and − 1.8, respectively (Supplementary Table S3).

4.2.3. Mafic granulite sample DHZ17

Zircons from the mafic granulite DHZ17 occur as anhedral grains. Their CL images exhibit well-developed oscillatory zoning as well as fir-tree zoning structures (Fig. 3c). Eighteen U–Pb–O analyses were performed on 16 zircons. They have highly variable U (114–1044 ppm) and Th (51–715 ppm) contents, with Th/U ratios of 0.29–0.69 (Supplementary Table S2). Analyses of the rim and core of the same zircon gave similar results within errors. Seventeen analyses define a cluster with a weighted mean $^{206}Pb/^{238}U$ age of 207 ± 3 Ma (MSWD = 2.9). Spot 5 yields a younger $^{206}Pb/^{238}U$ age of 193 ± 3 Ma (Fig. 4c). The analyzed zircons display slightly variable $\delta^{18}O$ values of 6.5–7.6‰ (Fig. 5a). In situ Hf isotopic analyses, performed on the same spots as U–Pb–O analyses, yield high $^{176}Hf/^{177}Hf$ ratios of 0.282658–0.282823, with corresponding positive $\varepsilon_{Hf}(t)$ values of +0.5 to +5.9 (Supplementary Table S3).

4.2.4. Felsic granulite sample DHZ19

Most zircons from the felsic granulite DHZ19 are anhedral and have cores and rims with either oscillatory or sector zoning (Fig. 3d). Most rims lack zoning, except for a few that exhibit irregular concentric zoning (Fig. 3d). Seventeen U–Pb–O isotopic analyses were performed on 12 zircons. They have highly variable Th (148–1483 ppm) and U (779–3719 ppm) contents with Th/U ratios of 0.06–0.53. Analyses of sector-zoned cores and rims without evident zoning yield $^{206}Pb/^{238}U$ apparent ages of 196 ± 3 to 226 ± 3 Ma; eight analyses define a cluster with a weighted mean $^{206}Pb/^{238}U$ age of 212 ± 2 Ma (MSWD = 0.91) (Fig. 4d). Analyses of oscillatory-zoned cores, on the other hand, yield $^{206}Pb/^{238}U$ apparent ages of 362 ± 5 to 429 ± 6 Ma (Supplementary Table S2, Fig. 4d). The analyzed zircons have relatively high $\delta^{18}O$ values of 6.8–7.6‰ (Supplementary Table S3). Nine in situ Hf isotopic analyses were performed on eight zircons on the same spots as U–Pb–O analyses. The analyzed zircons display low $^{176}Hf/^{177}Hf$ ratios of 0.282252–0.282442, with corresponding negative $\varepsilon_{Hf}(t)$ values of −6.1 to −12.6 (Supplementary Table S3; Fig. 5b, c).

5. Discussion

5.1. Formation and metamorphism of the Daoxian granulite xenoliths

Granulite xenoliths have been interpreted as being fragments of ancient lower crust, residues of crustal remelting, metamorphic cumulates derived from underplated melts, and metamorphic felsic rocks derived from partial melting of a pre-existing lower crust (Downes et al., 2007; Fan et al., 2005; Huang et al., 2001, 2004, 2013a; Jiang et al., 2011; Jiang and Guo, 2010; Liu et al., 2010; Wei et al., 2015; Zhou et al., 2002). The analyzed mafic granulite xenoliths have low SiO_2 (47.22–49.46 wt%) and high MgO (8.60–13.70 wt%) contents, suggesting that they originated from mantle-derived melts (Fig. 6). In the Mg# versus SiO_2/Al_2O_3 diagram (Fig. 6a), the Daoxian mafic granulite xenoliths display a tendency toward plagioclase accumulation, with higher Mg# values than the Hannuoba mafic granulite xenoliths, which are related to underplating of mafic melts (e.g., Fan et al., 2005; Kempton and Harmon, 1992; Liu et al., 2001; Zheng et al., 2009). Mesozoic zircons from the Daoxian mafic granulite xenoliths have variable $\varepsilon_{Hf}(t)$ values mainly in the range of −4.8 to +5.9, except for two extreme negative values of −17.3 and −19.2 (Fig. 5c). They all plot

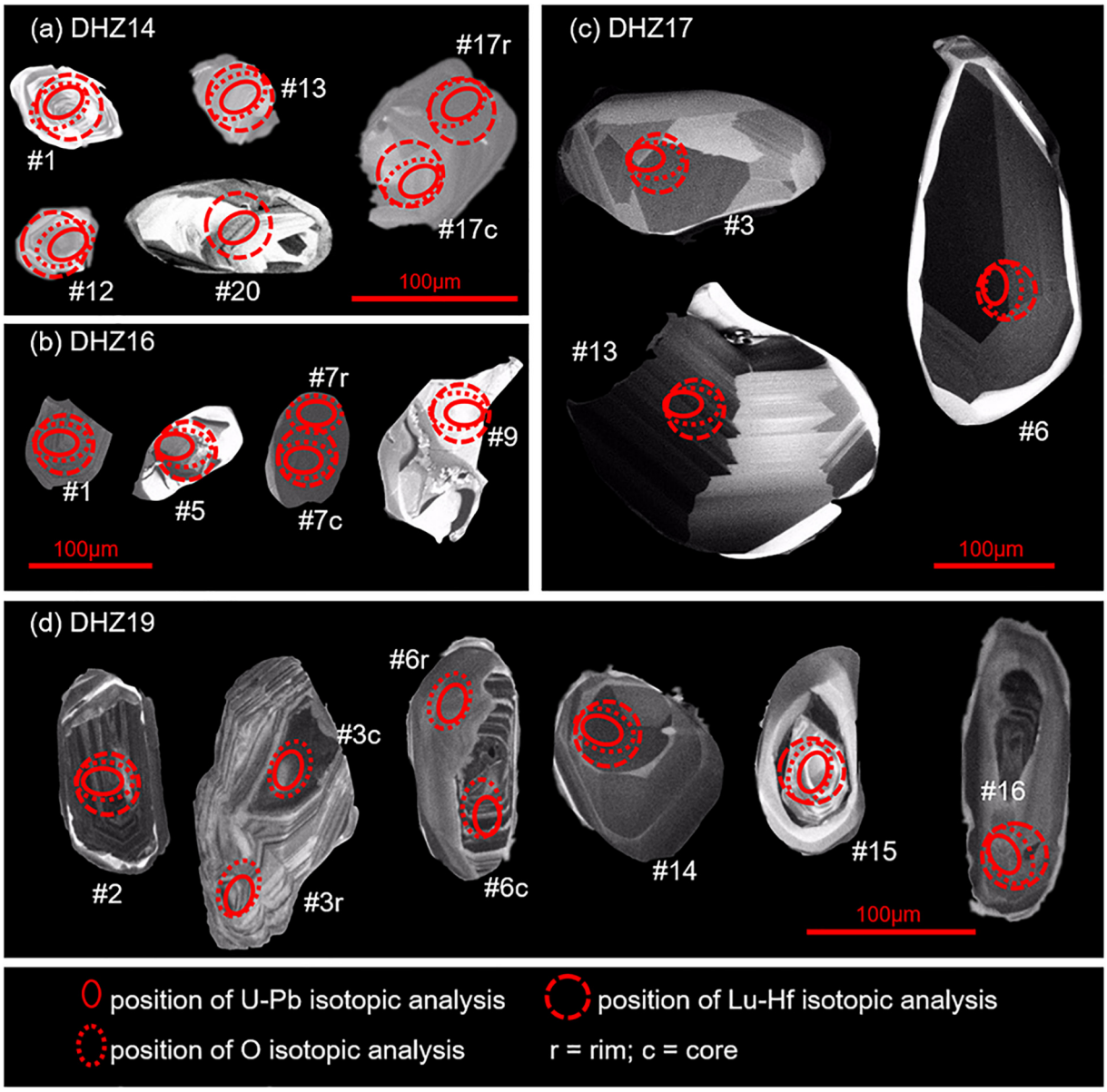

Fig. 3. Representative cathodoluminescence images of zircons from the Daoxian granulite xenoliths.

between the evolution lines of depleted mantle and average lower crust at 2.5 Ga (Fig. 5b). Furthermore, $\delta^{18}O$ values of these zircons (5.9–7.6‰) are higher than those of mantle-derived zircons (5.3 ± 0.3‰; Valley et al., 2005) but much lower than those of contemporaneous granitoids in the Cathaysia Block (Fig. 5a). Such zircon Hf—O isotopic compositions suggest that the protolith of Daoxian mafic granulite xenoliths was magmatic cumulates derived from a mantle source with variable contributions from crustal materials. This inference is consistent with mingling process related to magma underplating.

The youngest concordant ages (221–218 Ma) obtained from oscillatory-zoned zircons in mafic granulite samples DHZ14 and DHZ16 (Fig. 4a, b) represent the crystallization ages of their protoliths. In contrast, the fir-tree zoning structures of the zircons from the mafic granulite sample DHZ17 are the result of high-grade metamorphism with a weighted mean $^{206}Pb/^{238}U$ age of 207 ± 3 Ma. Furthermore, U—Pb ages of magmatic zircons from sample DHZ17 are indistinguishable from those of metamorphic zircons (Fig. 4c). Such overlap between magmatic and metamorphic ages suggests that the metamorphic event occurred immediately after magma underplating.

The analyzed felsic granulite xenoliths have high SiO_2 and low MgO contents (Fig. 6b), probably as a result of partial melting of crustal materials. Mesozoic zircons from the felsic granulite sample DHZ19 yield negative $\varepsilon_{Hf}(t)$ values (−7.3 to −12.6), which suggests a protolith of mainly old crustal materials, with a minor contribution from juvenile components (Fig. 5d). Moreover, the felsic granulite xenolith with low $\varepsilon_{Nd}(t)$ value (−11.4) and high initial $^{87}Sr/^{86}Sr$ ratio (0.7296) (Li et al., 2018) is very similar to the basement of South China. This resemblance indicates that felsic granulite might represent remelting product of old pre-existing crust. Mesozoic zircons from the felsic sample DHZ19 yield relatively constant $\varepsilon_{Hf}(t)$ values compared with those from mafic xenoliths (Fig. 5c), suggesting that the protolith of felsic granulites was derived from partial melting of crustal source rather than being a result of mingling processes.

Magma underplating usually results in the formation of juvenile crust and frequently induces the remelting of pre-existing lower crust (Downes et al., 1990, 1991; Fountain, 1989; Kempton et al., 1990; Ma et al., 2012; Thybo and Artemieva, 2013). Our data support these processes, as shown by some zircon U—Pb ages from the felsic granulite

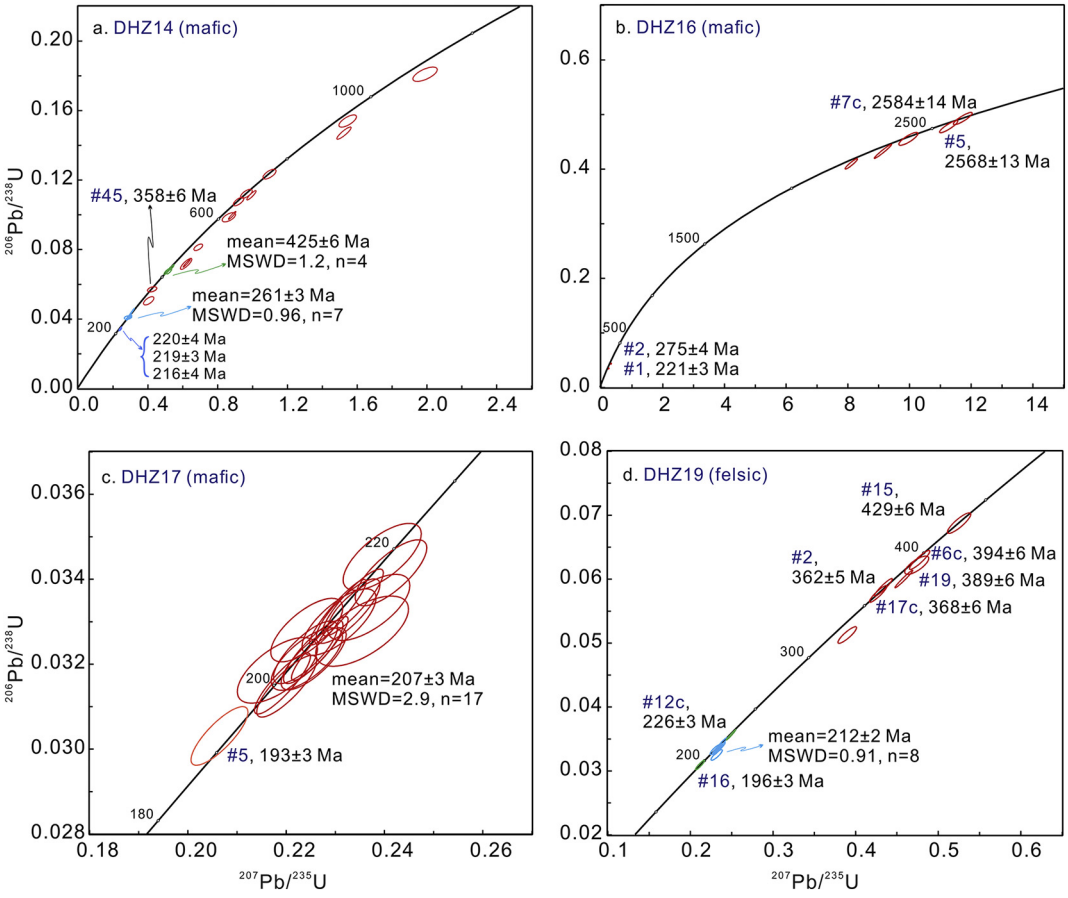

Fig. 4. U—Pb concordia diagrams of zircons from the Daoxian granulite xenoliths.

sample DHZ19 identical to those from mafic granulite samples. Spot 12 on the oscillatory-zoned core of a zircon from sample DHZ19 yields a $^{206}Pb/^{238}U$ age of 226 ± 3 Ma, whereas metamorphic zircons from the same sample yield $^{206}Pb/^{238}U$ ages of 218–196 Ma (Fig. 4d). These U—Pb ages are similar to those of crystallization (221–218 Ma) and metamorphism (218–193 Ma) recorded in the mafic granulite samples (Supplementary Table S2). Therefore, the Daoxian mafic and felsic granulite xenoliths are temporally associated, and both experienced successive events of magmatism and metamorphism. Although, the protolith of mafic granulites was derived from a mantle source, the protolith of felsic granulites was derived from the remelting of pre-existing lower crust.

5.2. Crustal accretion and reworking beneath the Cathaysia Block recorded by the Daoxian granulite xenoliths

Previous studies have shown that the Daoxian granulite xenoliths were transported from the lower crust by Mesozoic basalts (Li et al., 2004, 2018). Zircon U—Pb ages and Hf isotopic compositions obtained in this study, and data compiled from previous studies (Dai et al., 2008; Kong et al., 2016; Li et al., 2018), reveal that the xenoliths have an extremely complicated geochronology, which might provide information directly concerning the accretion and reworking history of the lower crust beneath the Cathaysia Block. The histogram of the zircon U—Pb ages from the granulite xenoliths indicates a wide range of ages (3126–193 Ma) with a degree of concordance of ≥90%, a significant peak at ca. 220 Ma and several small peaks during the Archean to the late Paleozoic (Fig. 7), indicating multistage accretion and reworking of the lower crust beneath the Cathaysia Block.

5.2.1. Late Archean juvenile crustal accretion

Due to the absence of Archean rocks, the ancient crustal materials in the Cathaysia Block have been debated for decades. However, U—Pb ages of the xenocrystic, inherited and detrital zircons, zircon Hf model ages, and whole-rock Nd model ages of some Phanerozoic rocks provide essential insights into the Archean basement (e.g., Chen and Jahn, 1998; Wan et al., 2007, 2010; Xu et al., 2007; Yu et al., 2010, 2012; Zheng et al., 2011). Archean geochronological data suggests that the Cathaysia Block underwent major episodes of crustal accretion at 2.8 and 2.6–2.5 Ga and minor episodes at 3.7–3.6 and 3.5–3.3 Ga, with crustal reworking occurring at 3.3–3.0 Ga (Yu et al., 2012). The mafic granulite xenoliths and their host basalts in the Daoxian region contain xenocrystic zircons that record late Archean U—Pb ages of 2.6–2.5 Ga (Dai et al., 2008; Li et al., 2018) and depleted Hf isotopic compositions ($\varepsilon_{Hf}(t) = +0.6$ to $+4.6$; Fig. 5b). Furthermore, depleted whole-rock Sr—Nd isotopic compositions have been reported for a late Archean mafic granulite xenolith (sample HZY09–37 in Li et al., 2018). Together, these data indicate accretion of juvenile crustal material beneath the Cathaysia Block at 2.6–2.5 Ga.

5.2.2. Proterozoic crustal reworking

Based on Precambrian detrital zircon U—Pb ages and Hf isotopic compositions, Li et al. (2014) proposed that accretion of juvenile crustal material beneath the Cathaysia Block occurred during the Paleo- to Mesoproterozoic crustal accretion (at ca. 1.85 and ca. 1.0 Ga, respectively) and that crustal reworking occurred during the Neoproterozoic. Zircons with Neoproterozoic ages (1191–659 Ma) are also reported in this study (Fig. 4) and might be related to the Neoproterozoic basement beneath the Cathaysia Block (e.g., Li et al., 2010; Shu et al., 2011; Wan et al., 2007, 2010). Additionally, analyzed Neoproterozoic zircons have sub-chondritic Hf isotopic compositions, old Hf model ages (up to

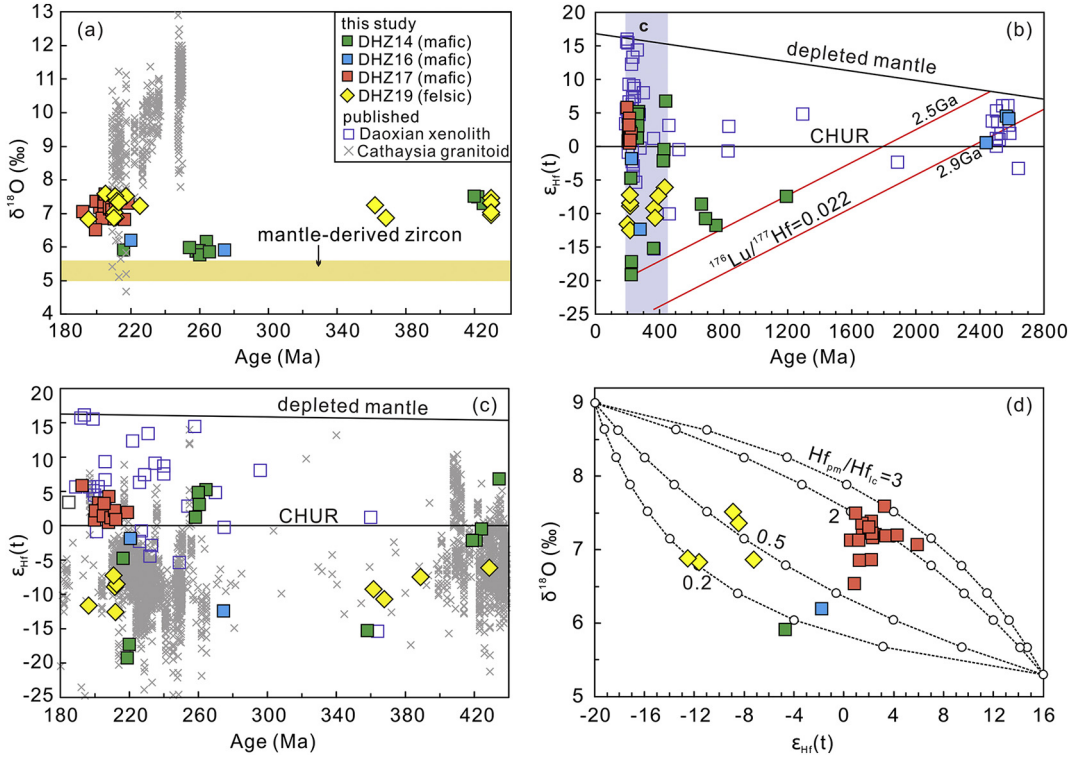

Fig. 5. Plots of (a) zircon $\delta^{18}O$ values versus U—Pb ages; (b, c) zircon $\varepsilon_{Hf}(t)$ values versus U—Pb ages; and (d) Mesozoic zircon $\delta^{18}O$ versus $\varepsilon_{Hf}(t)$ values. Zircon Hf—O isotopic data are from this study, Dai et al. (2008), Kong et al. (2016), Li et al. (2018) and references listed in the Supplementary Information. The dotted lines in (d) denote mixing trends between the depleted mantle- and lower-crust-derived magmas. Hf_{pm}/Hf_{lc} is the ratio of the Hf concentrations of a parental mantle magma (pm) and a lower crustal melt (lc), with the small open circles on the curves representing 10% mixing increments. The mantle is assumed to have a zircon $\varepsilon_{Hf}(t)$ value of +16 (represented by a Daoxian mafic granulite xenolith from Dai et al. (2008)) and a $\delta^{18}O$ value of 5.3‰ (Valley et al., 2005), while the zircon from the lower crust has an $\varepsilon_{Hf}(t)$ value of −20 (based on the mafic granulite DHZ14) and a $\delta^{18}O$ value of 9‰ (approximate average value of the Indosinian I-type granites in the Cathaysia Block).

2.5 Ga), and high $\delta^{18}O$ values (5.1–9.5‰) (Fig. 5b; Supplementary Table S3), indicating that crustal reworking rather than juvenile crustal generation was the primary process of crustal evolution beneath the Cathaysia Block during the Neoproterozoic. Crustal reworking might also have involved the recycling of Archean crustal materials.

5.2.3. Early Paleozoic crustal reworking and late Paleozoic crustal accretion

Paleozoic zircons from the Daoxian granulite xenoliths exhibit two clusters with $^{206}Pb/^{238}U$ ages of 425 ± 6 and 261 ± 3 Ma (Fig. 4a). Some early Paleozoic zircons yield relatively high $\varepsilon_{Hf}(t)$ values of up to +6.8, indicating the involvement of juvenile crustal materials. However, the relatively low $\varepsilon_{Hf}(t)$ values of most early Paleozoic zircons (−6.1 to −2.2; Fig. 5c) imply a contribution from recycled crustal materials, as further supported by the relatively high zircon $\delta^{18}O$ values (7.0–7.5‰; Fig. 5a). Moreover, the early Paleozoic igneous rocks in the Cathaysia Block are mainly peraluminous S-type granites, with subordinate I-type granites and scarce mafic rocks (Huang et al., 2013b;Shu et al., 2015; Wang et al., 2007, 2011; Yu et al., 2018), indicating significant contributions from remelting of crustal materials. Most of the S-type granites were derived from partial melting of the Proterozoic crustal basement without significant input from juvenile materials (Shu et al., 2015; Wang et al., 2007, 2011; Yu et al., 2018). I-type granites, on the other hand, were derived from partial melting of the middle–lower crust, with minor involvement of mantle materials (Huang et al., 2013b; Yu et al., 2018).

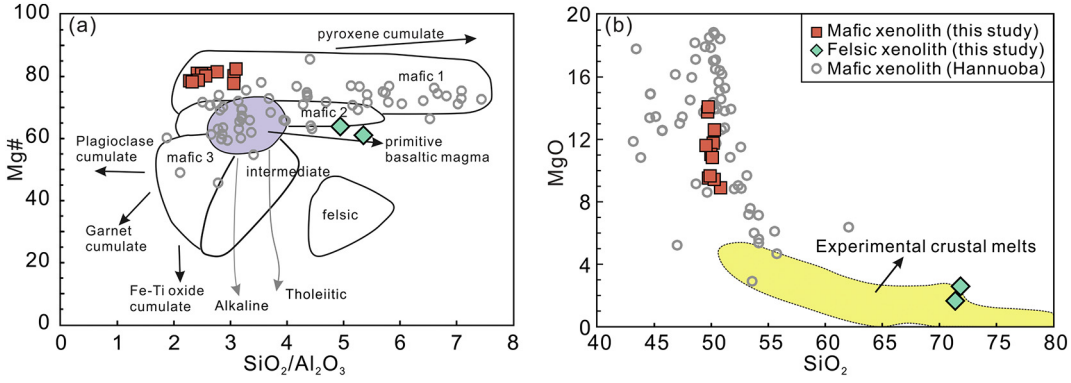

Fig. 6. Plots of (a) Mg# versus SiO_2/Al_2O_3 and (b) MgO versus SiO_2 for the Daoxian granulite xenoliths. Data for the Hannuoba xenoliths are shown for comparison and are from Fan et al. (2005), Huang et al. (2001), Jiang and Guo (2010), Jiang et al. (2011), Liu et al. (2001, 2005, 2010), Zhang et al. (1998), and Zheng et al. (2009). Data for experimental melts produced by partial melting of crustal rocks are from Gao et al. (2016).

In general, there is insufficient evidence to support the involvement of mantle-derived melts in crustal reworking processes beneath the Cathaysia Block during the early Paleozoic, except for the rare occurrence of gabbros, basalts, and MMEs (Wang et al., 2013; Xu and Xu, 2015; Yao et al., 2012; Zhang et al., 2015). In contrast, late Paleozoic (ca. 261 Ma) zircons from the Daoxian granulite xenoliths yield positive $\varepsilon_{Hf}(t)$ values (+1.3 to +5.3) and relatively low zircon $\delta^{18}O$ values (5.8–6.2‰), indicating a significant input of mantle-derived magmas. However, only a few outcrops of coeval igneous rocks, such as the Hainan Island shoshonitic intrusions (ca. 270 Ma) and I-type granites (262–269 Ma), occur in the Cathaysia Block (e.g., Li et al., 2006; Xie et al., 2006). The paucity of late Paleozoic magmatism in the Cathaysia Block indicates an overall quiescent period for crustal evolution (Xu et al., 1999). Summarizing, crustal reworking was the dominant process during the Paleozoic in the Cathaysia Block, while an input of mantle-derived magmas took place during the late Paleozoic.

5.2.4. Mesozoic crustal accretion and reworking

The late Triassic to early Jurassic zircons (226–193 Ma) from the Daoxian granulite xenoliths record their crystallization and metamorphic ages, and yield variable $\varepsilon_{Hf}(t)$ values (−19.2 to +5.9) and high $\delta^{18}O$ values (6.8–7.6‰) (Fig. 5a, c). The positive zircon $\varepsilon_{Hf}(t)$ values of the mafic sample DHZ17 (Fig. 5c) imply a significant input of mantle-derived magmas, consistent with the major element compositions of the mafic granulites. In particular, some late Triassic zircons from the Daoxian mafic crustal xenoliths exhibit very depleted Hf isotopic compositions with a highest $\varepsilon_{Hf}(t)$ value of +16 (Dai et al., 2008; Li et al., 2018), indicating significant juvenile crustal accretion. On the other hand, zircons with negative $\varepsilon_{Hf}(t)$ values (−19.2 to −1.8) suggest remelting of pre-existing crust. Our mixing model calculation using Hf—O isotopic compositions of Mesozoic zircons from mafic xenoliths indicates a significant contribution of variable proportions of pre-existing crust during magma underplating (Fig. 5d). Therefore, we propose that crustal accretion during the late Triassic was accompanied by significant reworking of pre-existing crustal materials. Granitoids contemporaneous with Daoxian crustal xenoliths are widespread in the Cathaysia Block (Fig. 1b), probably due to the intensive remelting of pre-existing crust. This inference is supported by the relatively evolved Hf and heavy O isotopic compositions of zircons from those granitoids (Fig. 5a, c).

5.3. Links between mantle-derived magmas and remelting of the lower crust

Phanerozoic igneous rocks in the Cathaysia Blockare mainly granitoids with minor mafic rocks (Fig. 8). The Phanerozoic granitoids were formed during three periods: the Caledonian (early Paleozoic), Indosinian (Triassic), and Yanshanian (Jurassic–Cretaceous) (e.g., Gao et al., 2017; Li and Li, 2007; Wang et al., 2011; Zhou et al., 2006). The radiogenic whole-rock Sr—Nd and zircon Hf isotopic data support the origin of these granitoids being the remelting of ancient curst (e.g., Chen and Jahn, 1998; Gao et al., 2016; Huang et al., 2013b; Wang et al., 2011). Mantle-derived melts also played an important role in the Cathaysia Block (e.g., Li et al., 2003, 2009; Wang et al., 2005, 2015; Xia et al., 2014; Yu et al., 2018). Previous studies have reported the shoshonitic syenites from the Fujian and Jiangxi provinces in the Cathaysia Block were derived from partial melting of a re-fertilized mantle source (Li et al., 2003; Wang et al., 2005), while granites in the Nanling Range of the block are associated with mantle-derived magma underplating (Li et al., 2009).

Magmatic zircons from the Phanerozoic granitoids in the Cathaysia Block display increasing $\varepsilon_{Hf}(t)$ and decreasing $\delta^{18}O$ values from the early to late Mesozoic (Fig. 9), implying a gradual increase in contributions from mantle-derived melts during the Yanshanian. Moreover, previous zircon U—Pb dating (Fig. 8) indicates relatively intensive Jurassic mafic magmatism in the Cathaysia Block; and previous K—Ar and ^{40}Ar—^{39}Ar dating indicates that the block experienced widespread basaltic magmatism during the Cretaceous (Wang et al., 2003). The presence of late Mesozoic–Cenozoic mafic granulite xenoliths in different localities (Qilin, Yingfengling, Xilong, and Mingxi) within the Cathaysia

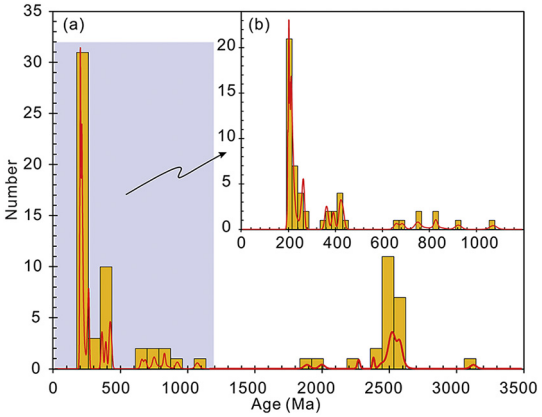

Fig. 7. Histogram of zircon U—Pb ages (discordance <10%) from the Daoxian granulite xenoliths. Data are from this study and Dai et al. (2008), Kong et al. (2016), and Li et al. (2018).

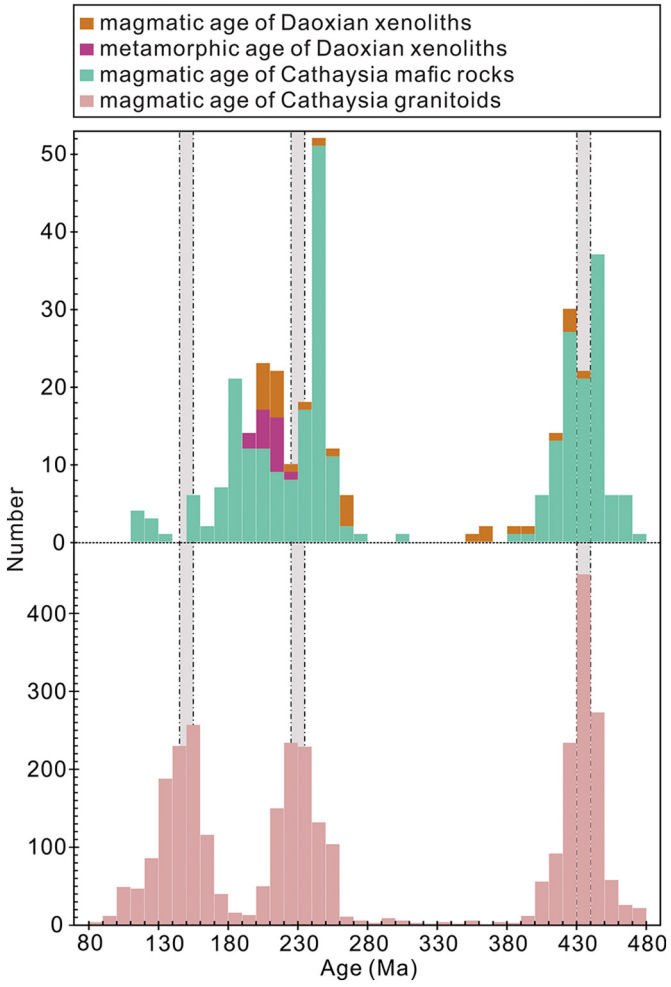

Fig. 8. Histogram of zircon U—Pb ages (discordance <10%) of the Daoxian granulite xenoliths and Phanerozoic igneous rocks in the Cathaysia Block. References are listed in the Supplementary Information. The method for calculating discordance used determined U—Pb ages as follows: discordance = $(1-t_{206/238}/t_{207/206}) \times 100\%$, t means age.

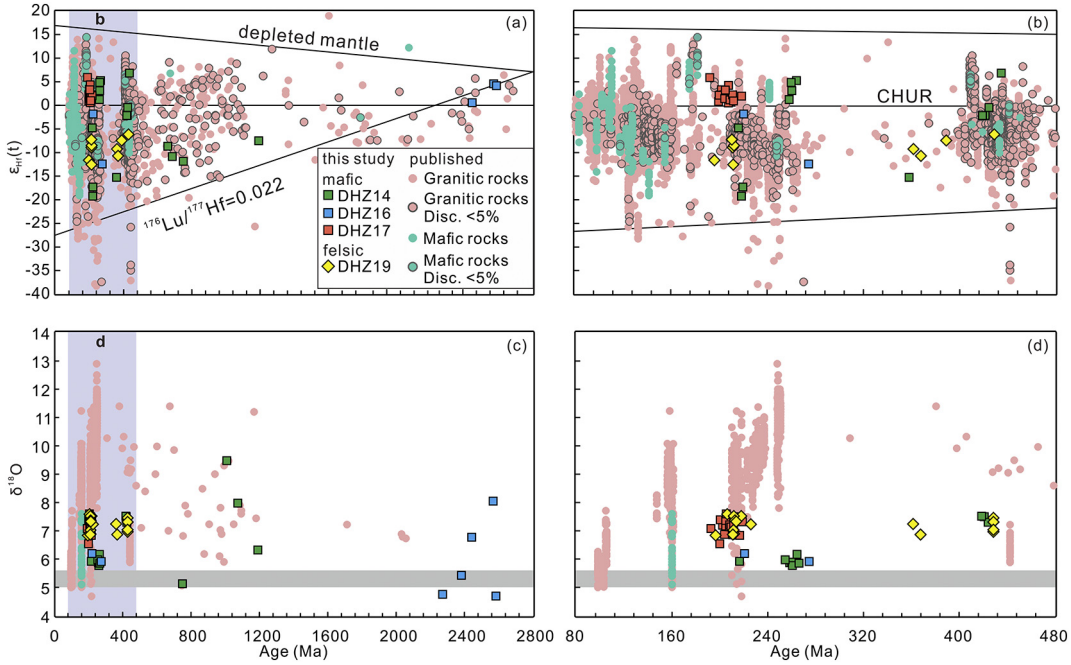

Fig. 9. Variation of zircon $\varepsilon_{Hf}(t)$ and $\delta^{18}O$ values with U—Pb ages of the Daoxian granulite xenoliths and Phanerozoic igneous rocks in the Cathaysia Block. References are listed in the Supplementary Information.

Block confirms the prevalent underplating of mafic magmas during the late Yanshanian (e.g., Huang et al., 2013a; Xu et al., 1999; Yu et al., 2003b). In addition, most mafic xenoliths and late Mesozoic basalts and gabbros in the Cathaysia Block have MORB-like to highly evolved Sr—Nd isotopic compositions (e.g., Gan et al., 2017; Jiang et al., 2015; Li et al., 2003, 2004; Wang et al., 2003; Yu et al., 2003b), suggesting binary mixing between crust and mantle due to magma underplating. Therefore, underplating of mantle-derived magmas during the late Mesozoic in the Cathaysia Block was an important mechanism, which might have triggered the remelting of crustal materials and thus caused extensive granitoid magmatism.

There is little evidence to support such a genetic relationship between magma underplating and intensive granitic magmatism in the early Paleozoic to early Mesozoic, mainly because of the scarcity of outcrops of mafic rocks in the Cathaysia Block. However, analyzed mafic materials such as MMEs, gabbros, and mafic dikes exhibit high MgO, Cr, and Ni contents and Mg# values, consistent with mantle-derived igneous rocks (e.g., Jiang et al., 2015; Wang et al., 2013; Xu and Xu, 2015; Zhang et al., 2015). Although mantle-derived mafic rocks from the early Mesozoic are volumetrically minor in SE China, geophysical data revealed an approximately five-km-thick layer of gabbro–basalt rocks at the lower part of the middle crust beneath the Cathaysia Block (Zhang et al., 2005, 2008), suggesting large-scale magma underplating in the early Yanshanian (Li et al., 2009). Furthermore, the zircon U—Pb ages and Hf—O isotopic compositions of early Mesozoic granulite xenoliths determined here indicate multistage accretion and reworking of the lower crust, consistent with the distribution of Phanerozoic igneous rocks in the Cathaysia Block (Figs. 8, 9). The Daoxian granulite xenoliths thus provide new information on the genetic relationship between magma underplating and crustal remelting in the Cathaysia Block during the early Yanshanian.

The Daoxian mafic and felsic granulite xenoliths were products of mantle-derived magma underplating and crustal remelting, respectively, according to their contrastive geochemical compositions. However, they experienced similar and successive magmatic and metamorphic events, suggesting a genetic relationship between the mafic and felsic rocks in the lower crust. It is noteworthy that early Indosinian granitoids older than the Daoxian crustal xenoliths (Fig. 8) are contemporaneous with the emplacement of intensive mafic rocks, which implies a genetic relationship between mafic and felsic rocks in the early Indosinian. We propose that magma underplating recorded by the Daoxian mafic granulite xenoliths may have provided the necessary heat for remelting of pre-existing lower crust, contributing to the formation of the late Triassic to Jurassic granitoids in the Cathaysia Block.

6. Conclusions

The Daoxian mafic and felsic granulite xenoliths record successive magmatic (226–218 Ma) and metamorphic (218–193 Ma) events. The mafic granulites were formed mainly through underplating of mantle-derived magmas, whereas the felsic granulites originated from remelting of pre-existing lower crust.

The Daoxian granulite xenoliths record the multistage evolution of the lower crust beneath the Cathaysia Block, including crustal reworking during the early Paleozoic and magma underplating during the early Mesozoic. Magma underplating triggered the remelting of pre-existing crustal materials, resulting in widespread Mesozoic granitoid magmatism in the Cathaysia Block.

Supplementary data to this article can be found online at https://doi.org/10.1016/j.lithos.2020.105596.

Declaration of Competing Interest

The authors declare that they have no known competing financial interests or personal relationships that could have appeared to influence the work reported in this paper.

Acknowledgement

We appreciated greatly Q. Yang, Y.N. Yang, X.P. Xia, L. Zhang and L.R. Tian for assistance with in situ analyses on zircons and whole rocks major oxides analyses. We gratefully acknowledge the constructive comments of two anonymous reviewers, which considerably improved this contribution, and appreciate Prof. X.H. Li for his constructive comments and editorial handling. This study was financially supported by

National Natural Science Foundation of China (NSFC Projects 41625007, 41903033, U1701641, 41890812). This is contribution No. IS-2870 from GIG-CAS.

References

Chen, J.F., Jahn, B.M., 1998. Crustal evolution of southeastern China: Nd and Sr isotopic evidence. Tectonophysics 284, 101–133.

Chen, W.F., Chen, P.R., Huang, H.Y., Ding, X., Sun, T., 2007. Chronological and geochemical studies of granite and enclave in Baimashan pluton, Hunan, South China. Sci. China Ser. D Earth Sci. 50 (11), 1606–1627.

Chen, Q., Sun, M., Long, X.P., Zhao, G.C., Wang, J., Yu, Y., Yuan, C., 2018. Provenance study for the Paleozoic sedimentary rocks from the West Yangtze Block: constraint on possible link of South China to the Gondwana supercontinent reconstruction. Precambrian Res. 309, 271–289.

Dai, B.Z., Jiang, S.Y., Jiang, Y.H., Zhao, K.D., Liu, D.Y., 2008. Geochronology, geochemistry and Hf–Sr–Nd isotopic compositions of Huziyan mafic xenoliths, southern Hunan province, South China: petrogenesis and implications for lower crust evolution. Lithos 102 (1), 65–87.

Downes, H., Dupuy, C., Leyreloup, A.F., 1990. Crustal evolution of the Hercynian belt of Western Europe: evidence from lower-crustal granulitic xenoliths (French Massif Central). Chem. Geol. 83 (3–4), 209–231.

Downes, H., Kempton, P.D., Briot, D., Harmon, R.S., Leyreloup, A.F., 1991. Pb and O isotope systematics in granulite facies xenoliths, French Massif Central: implications for crustal processes. Earth Planet. Sci. Lett. 102 (3–4), 342–357.

Downes, H., Upton, B.G.J., Connolly, J., Beard, A.D., Bodinier, J.L., 2007. Petrology and geochemistry of a cumulate xenolith suite from Bute: evidence for late Palaeozoic crustal underplating beneath SW Scotland. J. Geol. Soc. Lond. 164 (6), 1217–1231.

Fan, Q.C., Zhang, H.F., Sui, J.L., Zhai, M.G., Sun, Q., Li, N., 2005. Magma underplating and Hannuoba present crust-mantle transitional zone composition: Xenolith petrological and geochemical evidence. Sci. China Ser. D Earth Sci. 48, 1089–1105.

Fountain, D.M., 1989. Growth and modification of lower continental crust in extended terrains: the role of extension and magmatic underplating. Properties and processes of earth's lower crust. American Geophysical Union (AGU) 51, 287–299.

Fyfe, W.S., 1992. Magma underplating of continental crust. J. Volcanol. Geotherm. Res. 50 (1), 33–40.

Gan, C.S., Wang, Y.J., Qian, X., Bi, M.W., He, H.Y., 2017. Constraints of the Xialan gabbroic intrusion in the Eastern Nanling Range on the early Jurassic intra-continental extension in eastern South China. J. Asian Earth Sci. 145, 576–590.

Gao, P., Zheng, Y.F., Zhao, Z.F., 2016. Experimental melts from crustal rocks: a lithochemical constraint on granite petrogenesis. Lithos 266–267, 133–157.

Gao, P., Zheng, Y.F., Zhao, Z.F., 2017. Triassic granites in South China: a geochemical perspective on their characteristics, petrogenesis, and tectonic significance. Earth Sci. Rev. 173, 266–294.

Huang, X.L., Xu, Y.G., Chu, X.L., Zhang, H.X., Liu, C.Q., 2001. Geochemical comparative studies of some granulite terranes and granulite xenoliths from North China Craton. Acta Petrol. Mineral. 20 (3), 318–329 (in Chinese with English abstract).

Huang, X.L., Xu, Y.G., Liu, D.Y., 2004. Geochronology, petrology and geochemistry of the granulite xenoliths from Nushan, East China: implication for a heterogeneous lower crust beneath the Sino-Korean Craton. Geochim. Cosmochim. Acta 68 (1), 127–149.

Huang, X.L., Zhong, J.W., Yu, Y., Li, J., 2013a. Geochronology and mineralogy of the Mingxi granulite xenoliths from Fujian, South China: geotherm and implications for the Mesozoic crustal-mantle interaction. Bull. Mineral. Petrol. Geochem. 32 (2), 212–222 (in Chinese with English abstract).

Huang, X.L., Yu, Y., Li, J., Tong, L.X., Chen, L.L., 2013b. Geochronology and petrogenesis of the early Paleozoic I-type granite in the Taishan area, South China: middle-lower crustal melting during orogenic collapse. Lithos 177, 268–284.

Jiang, N., Guo, J.H., 2010. Hannuoba intermediate-mafic granulite xenoliths revisited: assessment of a Mesozoic underplating model. Earth Planet. Sci. Lett. 293 (3–4), 277–288.

Jiang, N., Carlson, R.W., Guo, J.H., 2011. Source of mesozoic intermediate-felsic igneous rocks in the North China Craton: granulite xenolith evidence. Lithos 125 (1–2), 335–346.

Jiang, Y.H., Wang, G.C., Liu, Z., Ni, C.Y., Qing, L., Zhang, Q., 2015. Repeated slab advance-retreat of the Palaeo-Pacific plate underneath SE China. Int. Geol. Rev. 57 (4), 472–491.

Kempton, P.D., Harmon, R.S., 1992. Oxygen isotope evidence for large-scale hybridization of the lower crust during magmatic underplating. Geochim. Cosmochim. Acta 56, 971–986.

Kempton, P.D., Harmon, R.S., Hawkesworth, C.J., Moorbath, S., 1990. Petrology and geochemistry of lower crustal granulites from the Geronimo Volcanic Field, Southeastern Arizona. Geochim. Cosmochim. Acta 54 (12), 3401–3426.

Kong, H., Xu, M.Z., Zhang, Q., Tang, Y.Q., Zhao, J.J., 2016. LA–ICP–MS Zircon U–Pb dating and Hf isotope feature of gabbro xenolith and its geological significance in Huziyan basalt of Daoxian county, Southern Hunan Province. J. Jilin Univ. 46 (3), 627–638 (in Chinese with English abstract).

Li, Z.X., Li, X.H., 2007. Formation of the 1300-km-wide intracontinental orogen and postorogenic magmatic province in Mesozoic South China: a flat-slab subduction model. Geology 35 (2), 179–182.

Li, X.H., Tatsumoto, M., Premo, W.R., Gui, X.T., 1989. Age and origin of the Tanghu granite, Southeast China: results from U–Pb single zircon and Nd isotopes. Geology 17 (5), 395–399.

Li, X.H., Liu, D.Y., Li, W.X., 2003. Jurassic Gabbro–granite–syenite suites from Southern Jiangxi Province, SE China: age, origin, and tectonic significance. Int. Geol. Rev. 45 (10), 898–921.

Li, X.H., Chung, S.L., Zhou, H.W., Lo, C.H., Liu, Y., Chen, C.H., 2004. Jurassic intraplate magmatism in southern Hunan–eastern Guangxi: 40Ar/39Ar dating, geochemistry, Sr–Nd isotopes and implications for the tectonic evolution of SE China. Geol. Soc. Lond. Spec. Publ. 226, 193–215.

Li, X.H., Li, Z.X., Li, W.X., Wang, Y.J., 2006. Initiation of the Indosinian orogeny in South China: evidence for a Permian magmatic arc on Hainan Island. J. Geol. 114 (3), 341–353.

Li, X.H., Li, W.X., Wang, X.C., Li, Q.L., Liu, Y., Tang, G.Q., 2009. Role of mantle-derived magma in genesis of early Yanshanian granites in the Nanling range, South China: in situ zircon Hf–O isotopic constraints. Sci. China Ser. D Earth Sci. 52 (9), 1262–1278.

Li, Z.X., Li, X.H., Wartho, J.A., Clark, C., Li, W.X., Zhang, C.L., Bao, C.D., 2010. Magmatic and metamorphic events during the early Paleozoic Wuyi-Yunkai orogeny, southeastern South China: new age constraints and pressure–temperature conditions. Geol. Soc. Am. Bull. 122 (5–6), 772–793.

Li, X.H., Li, Z.X., Li, W.X., 2014. Detrital zircon U–Pb age and Hf isotope constrains on the generation and reworking of Precambrian continental crust in the Cathaysia Block, South China: a synthesis. Gondwana Res. 25 (3), 1202–1215.

Li, X.Y., Zheng, J.P., Xiong, Q., Zhou, X., Xiang, L., 2018. Triassic rejuvenation of unexposed Archean–Paleoproterozoic deep crust beneath the western Cathaysia Block, South China. Tectonophysics 724–725, 65–79.

Liu, Y.S., Gao, S., Jin, S.Y., Hu, S.H., Sun, M., Zhao, Z.B., Feng, J.L., 2001. Geochemistry of lower crustal xenoliths from Neogene Hannuoba Basalt, North China Craton: Implications for petrogenesis and lower crustal composition. Geochim. Cosmochim. Acta 65 (15), 2589–2604.

Liu, Y.S., Gao, S., Lee, C.A., Hu, S.H., Liu, X.M., Huan, H.L., 2005. Melt-peridotite interactions: links between garnet pyroxenite and high-Mg# signature of continental crust. Earth Planet. Sci. Lett. 234, 39–57.

Liu, Y.S., Gao, S., Gao, C.G., Zong, K.Q., Hu, Z.C., Ling, W.L., 2010. Garnet-rich granulite xenoliths from the Hannuoba basalts, North China: petrogenesis and implications for the Mesozoic crust-mantle interaction. J. Earth Sci. 21 (5), 669–691.

Ma, Q., Zheng, J.P., Griffin, W.L., Zhang, M., Tang, H.Y., Su, Y.P., Ping, X.Q., 2012. Triassic "adakitic" rocks in an extensional setting (North China): Melts from the cratonic lower crust. Lithos 149, 159–173.

Moyen, J.F., Paquette, J.L., Ionov, D.A., Gannoun, A., Korsakov, A.V., Golovin, A.V., Moine, B.N., 2017. Paleoproterozoic rejuvenation and replacement of Archaean lithosphere: evidence from zircon U–Pb dating and Hf isotopes in crustal xenoliths at Udachnaya, Siberian craton. Earth Planet. Sci. Lett. 457, 149–159.

Rudnick, R.L., 1995. Making continental crust. Nature 378, 571–578.

Shu, L.S., Faure, M., Yu, J.H., Jahn, B.M., 2011. Geochronological and geochemical features of the Cathaysia block (South China): new evidence for the Neoproterozoic breakup of Rodinia. Precambrian Res. 187, 263–276.

Shu, L.S., Wang, B., Cawood, P.A., Santosh, M., Xu, Z.Q., 2015. Early Paleozoic and early Mesozoic intraplate tectonic and magmatic events in the Cathaysia Block, South China. Tectonics 34 (8), 1600–1621.

Thybo, H., Artemieva, I.M., 2013. Moho and magmatic underplating in continental lithosphere. Tectonophysics 609, 605–619.

Valley, J.W., Lackey, J.S., Cavosie, A.J., Clechenko, C.C., Spicuzza, M.J., Basei, M.A.S., Bindeman, I.N., Ferreira, V.P., Sial, A.N., King, E.M., Peck, W.H., Sinha, A.K., Wei, C.S., 2005. 4.4 billion years of crustal maturation: Oxygen isotope ratios of magmatic zircon. Contrib. Mineral. Petrol. 150, 561–580.

Wan, Y.S., Liu, D.Y., Xu, M.H., Zhuang, J.M., Song, B., Shi, Y.R., Du, L.L., 2007. SHRIMP U–Pb zircon geochronology and geochemistry of metavolcanic and metasedimentary rocks in Northwestern Fujian, Cathaysia block, China: tectonic implications and the need to redefine lithostratigraphic units. Gondwana Res. 12 (1–2), 166–183.

Wan, Y.S., Liu, D.Y., Wilde, S., Cao, J.J., Chen, B., Dong, C.Y., Song, B., Du, L.L., 2010. Evolution of the Yunkai Terrane, South China: evidence from SHRIMP zircon U–Pb dating, geochemistry and Nd isotope. J. Asian Earth Sci. 37 (2), 140–153.

Wang, Y.J., Fan, W.M., Guo, F., Peng, T.P., Li, C.W., 2003. Geochemistry of Mesozoic mafic rocks adjacent to the Chenzhou–Linwu Fault, South China: implications for the lithospheric boundary between the Yangtze and Cathaysia Blocks. Int. Geol. Rev. 45 (3), 263–286.

Wang, Q., Li, J.W., Jian, P., Zhao, Z.H., Xiong, X.L., Bao, Z.W., Xu, J.F., Li, C.F., Ma, J.L., 2005. Alkaline syenites in eastern Cathaysia (South China): link to Permian–Triassic transtension. Earth Planet. Sci. Lett. 230, 339–354.

Wang, Y.J., Fan, W.M., Sun, M., Liang, X.Q., Zhang, Y.H., Peng, T.P., 2007. Geochronological, geochemical and geothermal constraints on petrogenesis of the Indosinian peraluminous granites in the South China Block: a case study in the Hunan Province. Lithos 96 (3), 475–502.

Wang, Y.J., Zhang, A.M., Fan, W.M., Zhao, G.C., Zhang, G.W., Zhang, Y.Z., Zhang, F.F., Li, S.Z., 2011. Kwangsian crustal anatexis within the eastern South China Block: Geochemical, zircon U–Pb geochronological and Hf isotopic fingerprints from the gneissoid granites of Wugong and Wuyi–Yunkai Domains. Lithos 127 (1–2), 239–260.

Wang, Y.J., Zhang, A.M., Fan, W.M., Zhang, Y.H., Zhang, Y.Z., 2013. Origin of paleosubduction-modified mantle for Silurian gabbro in the Cathaysia Block: geochronological and geochemical evidence. Lithos 160–161, 37–54.

Wang, K.X., Chen, W.F., Chen, P.R., Ling, H.F., Huang, H., 2015. Petrogenesis and geodynamic implications of the Xiema and Ziyunshan plutons in Hunan Province, South China. J. Asian Earth Sci. 111, 919–935.

Wei, Y., Zheng, J.P., Su, Y.P., Ma, Q., Griffin, W.L., 2015. Lithological and age structure of the lower crust beneath the northern edge of the North China Craton: xenolith evidence. Lithos 216–217, 211–223.

Xia, Y., Xu, X.S., Zou, H.B., Liu, L., 2014. Early Paleozoic crust-mantle interaction and lithosphere delamination in South China Block: evidence from geochronology, geochemistry, and Sr–Nd–Hf isotopes of granites. Lithos 184–187, 416–435.

Xiang, L., Zheng, J.P., Siebel, W., Griffin, W.L., Wang, W., O'Reilly, S.Y., Li, Y.H., Zhang, H., 2018. Unexposed Archean components and complex post-Archean accretion/

reworking processes beneath the southern Yangtze Block revealed by zircon xenocrysts from Paleozoic lamproites, South China. Precambrian Res. 316, 174–196.
Xie, C.F., Zhu, J.C., Ding, S.J., 2006. Identification of Hercynian shoshonitic intrusive rocks in Central Hainan Island and its geotectonic implications. Chin. Sci. Bull. 51 (20), 2507–2519 (in Chinese with English abstract).
Xu, W.J., Xu, X.S., 2015. Early Paleozoic intracontinental felsic magmatism in the South China Block: petrogenesis and geodynamics. Lithos 234–235, 79–92.
Xu, X.S., Zhou, X.M., O'Reilly, S.Y., Tang, H.F., 1999. Exploration for the lower crustal materials and granite genesis in Southeast China. Acta Petrol. Sin. 15 (2), 217–223 (in Chinese with English abstract).
Xu, X.S., O'Reilly, S.Y., Griffin, W.L., Wang, X.L., Pearson, N.J., He, Z.Y., 2007. The crust of Cathaysia: age, assembly and reworking of two terranes. Precambrian Res. 158 (1–2), 51–78.
Yan, D.P., Zhou, M.F., Song, H.L., Wang, X.W., Malpas, J., 2003. Origin and tectonic significance of a Mesozoic multi-layer over-thrust system within the Yangtze Block (South China). Tectonophysics 361 (3–4), 239–254.
Yang, Q., Xia, X.P., Zhang, W.F., Zhang, Y.Q., Xiong, B.Q., Xu, Y.G., Wang, Q., Wei, G.J., 2018. An evaluation of precision and accuracy of SIMS oxygen isotope analysis. Solid Earth Sci. 3, 81–86.
Yao, W.H., Li, Z.X., Li, W.X., Wang, X.C., Li, X.H., Yang, J.H., 2012. Post-kinematic lithospheric delamination of the Wuyi-Yunkai orogen in South China: evidence from ca. 435 Ma high–Mg basalts. Lithos 154, 115–129.
Yu, J.H., Xu, X.S., O'Reilly, S.Y., Griffin, W.L., Zhang, M., 2003a. Granulite xenoliths from Cenozoic Basalts in SE China provide geochemical fingerprints to distinguish lower crust terranes from the North and South China tectonic blocks. Lithos 67 (1–2), 77–102.
Yu, J.H., Xu, X.S., Zhou, X.M., 2003b. Late Mesozoic crust-mantle interaction and lower crust components in South China: a geochemical study of mafic granulite xenoliths from Cenozoic basalts. Sci. China Ser. D Earth Sci. 5, 447–460.
Yu, J.H., O'Reilly, S.Y., Wang, L.J., Griffin, W.L., Zhou, M.F., Zhang, M., Shu, L.S., 2010. Components and episodic growth of Precambrian crust in the Cathaysia Block, South China: evidence from U–Pb ages and Hf isotopes of zircons in Neoproterozoic sediments. Precambrian Res. 181 (1–4), 97–114.
Yu, J.H., O'Reilly, S.Y., Zhou, M.F., Griffin, W.L., Wang, L.J., 2012. U–Pb geochronology and Hf–Nd isotopic geochemistry of the Badu complex, Southeastern China: implications for the Precambrian crustal evolution and paleogeography of the Cathaysia Block. Precambrian Res. 222–223, 424–449.
Yu, Y., Huang, X.L., Sun, M., He, P.L., 2018. Petrogenesis of granitoids and associated xenoliths in the early Paleozoic Baoxu and Enping plutons, South China: Implications for the evolution of the Wuyi–Yunkai intracontinental orogen. J. Asian Earth Sci. 156, 59–74.
Zhang, G.H., Zhou, X.H., Sun, M., Chen, S.H., Feng, J.L., 1998. Highly chemical heterogeneity in the lower crustal and crust-mantle transitional zone: geochemical evidences from xenoliths in Hannuoba basalt, Hebei Province. Geochimica 27 (2), 153–169 (in Chinese with English abstract).
Zhang, Z.J., Badal, J., Li, Y.K., Chen, Y., Yang, L.Q., Teng, J.W., 2005. Crust-upper mantle seismic velocity structure across Southeastern China. Tectonophysics 395, 137–157.
Zhang, Z.J., Zhang, X., Badal, J., 2008. Composition of the crust beneath southeastern China derived from an integrated geophysical data set. J. Geophys. Res. 113, B04417.
Zhang, Q., Jiang, Y.H., Wang, G.C., Liu, Z., Ni, C.Y., Qing, L., 2015. Origin of Silurian gabbros and I-type granites in Central Fujian, SE China: implications for the evolution of the early Paleozoic orogen of South China. Lithos 216–217, 285–297.
Zhao, G.C., Cawood, P.A., 2012. Precambrian geology of China. Precambrian Res. 222–223, 13–54.
Zhao, J.H., Li, Q.W., Liu, H., Wang, W., 2018. Neoproterozoic magmatism in the western and northern margins of the Yangtze Block (South China) controlled by slab subduction and subduction-transform-edge-propagator. Earth Sci. Rev. 187, 1–18.
Zheng, J.P., O'Reilly, S.Y., Griffin, W.L., Zhang, M., Lu, F.X., Liu, G.L., 2004. Nature and evolution of Mesozoic-Cenozoic lithospheric mantle beneath the Cathaysia block, SE China. Lithos 74, 41–65.
Zheng, J.P., Griffin, W.L., O'Reilly, S.Y., Zhang, M., Pearson, N., Pan, Y.M., 2006. Widespread Archean basement beneath the Yangtze craton. Geology 34 (6), 417–420.
Zheng, J.P., Griffin, W.L., Qi, L., O'Reilly, S.Y., Sun, M., Zheng, S., Pearson, N., Gao, J.F., Yu, C.M., Su, Y.P., Tang, H.Y., Liu, Q.S., Wu, X.L., 2009. Age and composition of granulite and pyroxenite xenoliths in Hannuoba basalts reflect Paleogene underplating beneath the North China Craton. Chem. Geol. 264 (1–4), 266–280.
Zheng, J.P., Griffin, W.L., Li, L.S., O'Reilly, S.Y., Pearson, N.J., Tang, H.Y., Liu, G.L., Zhao, J.H., Yu, C.M., Su, Y.P., 2011. Highly evolved Archean basement beneath the western Cathaysia Block, South China. Geochim. Cosmochim. Acta 75 (1), 242–255.
Zhong, Y.F., Ma, C.Q., Zhang, C., Wang, S.M., She, Z.B., Liu, L., Xu, H.J., 2013. Zircon U–Pb age, Hf isotopic compositions and geochemistry of the Silurian Fengdingshan I-type granite Pluton and Taoyuan mafic–felsic complex at the southeastern margin of the Yangtze Block. J. Asian Earth Sci. 74, 11–24.
Zhou, X.M., Li, W.X., 2000. Origin of late Mesozoic igneous rocks in Southeastern China: implications for lithosphere subduction and underplating of mafic magmas. Tectonophysics 326, 269–287.
Zhou, X.H., Sun, M., Zhang, G.H., Chen, S.H., 2002. Continental crust and lithospheric mantle interaction beneath North China: isotopic evidence from granulite xenoliths in Hannuoba, Sino–Korean craton. Lithos 62 (3–4), 111–124.
Zhou, X.M., Sun, T., Shen, W.Z., Shu, L.S., Niu, Y.L., 2006. Petrogenesis of Mesozoic granitoids and volcanic rocks in South China: a response to tectonic evolution. Episodes 29 (1), 26–33.